AIP | The Journal of Chemical Physics

New CO–CO interaction potential tested by rovibrational calculations

G. W. M. Vissers, A. Heßelmann, G. Jansen, P. E. S. Wormer, and A. van der Avoird

Citation: J. Chem. Phys. **122**, 054306 (2005); doi: 10.1063/1.1835262
View online: http://dx.doi.org/10.1063/1.1835262
View Table of Contents: http://jcp.aip.org/resource/1/JCPSA6/v122/i5
Published by the American Institute of Physics.

New CO–CO interaction potential tested by rovibrational calculations

G. W. M. Vissers
Institute of Theoretical Chemistry, NSRIM, University of Nijmegen, Toernooiveld 1, 6525 ED Nijmegen, The Netherlands

A. Heßelmann and G. Jansen
Theoretische Organische Chemie, Institut für Organische Chemie, Universität Duisburg-Essen, Campus Essen, Universitätsstr. 5, D-45117 Essen, Germany

P. E. S. Wormer and A. van der Avoird[a)]
Institute of Theoretical Chemistry, NSRIM, University of Nijmegen, Toernooiveld 1, 6525 ED Nijmegen, The Netherlands

(Received 19 August 2004; accepted 29 October 2004; published online 18 January 2005)

A four-dimensional potential energy surface (PES) for the CO dimer consisting of rigid molecules has been calculated, using a scheme that combines density functional theory to describe the monomers and symmetry adapted perturbation theory for the interaction energy (DFT-SAPT). The potential is fitted in terms of analytic functions, and the fitted potential is used to compute the lowest rovibrational states of the dimer. The quality of the PES is comparable to that of a previously published surface [G. W. M. Vissers, P. E. S. Wormer, and A. van der Avoird, Phys. Chem. Chem. Phys., **5**, 4767 (2003)], which was calculated with the coupled cluster single double and perturbative triples [CCSD(T)] method. It is shown that a weighted average of the DFT-SAPT and the CCSD(T) potential gives results that are in very good agreement with experimental data, for both $(^{12}CO)_2$ and $(^{13}CO)_2$. The relative weight was determined by adjusting the energy gap between the origins of the lowest two stacks of rotational levels of $(^{12}CO)_2$ to the measured value. © *2005 American Institute of Physics.* [DOI: 10.1063/1.1835262]

I. INTRODUCTION

The molecule carbon monoxide is abundant: it appears in the earth's atmosphere as well as in interstellar clouds. Because of the possibility of dimer formation, the CO dimer has been the subject of several theoretical and experimental studies.[1–3] It is a prototype of weakly bound van der Waals molecules. The spectra of van der Waals complexes provide accurate information on intermolecular potentials and the CO dimer is an interesting example, because the *ab initio* calculation of an accurate CO–CO potential energy surface turned out to be more difficult than for other systems.[4–6]

Work on the CO dimer dates back as far as 1979, when Vanden Bout *et al.* reported the observation of five lines due to $(CO)_2$ in a molecular beam radiospectroscopic measurement.[1] Although these lines still remain unassigned, much experimental knowledge has been gained about this system since then. Havenith *et al.*[2] reported studies of the dimer in the midinfrared, and analyzed their results in terms of an asymmetric rigid rotor model. This analysis was later rejected by Brookes and McKellar,[3,7] who described the dimer rather as consisting of two hindered rotors. Millimeter wave experiments added to the body of knowledge, to the point that there are now several stacks of accurately known rovibrational energy levels, both for the ''normal'' $(^{12}CO)_2$ (Refs. 8–12) and for the isotopically substituted $(^{13}CO)_2$.[13,14]

On the theoretical side of the problem, progress was considerably slower. Until recently, there were only two *ab initio* potential energy surfaces (PESs) available. The first, by van der Pol *et al.*[15] is a sum of first-order Heitler-London energy and a damped multipole expansion for the electrostatic, induction and dispersion interactions. The second surface, by Meredith and Stone[16] is an extension of the potential of van der Pol. They included C_9 and C_{10} coefficients in the multipole expansion of the dispersion energy, and refined the electrostatic and induction energies by using distributed multipoles. Both potentials show a global minimum at or near a T-shaped structure, and local minima corresponding to slipped antiparallel structures. However, rovibrational calculations on these potentials showed that neither of them can explain the observed spectroscopic properties of the CO dimer.[16,17]

Two possible reasons for the inaccuracies of these potentials are the use of the multipole approximation and the neglect of electronic correlation effects on the exchange-repulsion energy. However, an attempt[4] to correct these deficiencies by fourth-order Møller-Plesset and coupled cluster (CC) calculations showed that high-order correlation effects are important, and that both CCSD(T) (CC restricted to single, double, and noniterative triple excitations) and CCSDT (CC with iterative triple excitations) do not have the correct asymptotic behavior. Furthermore, it was pointed out that very large basis sets are needed for an accurate description of the CO–CO potential energy surface.[5,6] Nevertheless, a CCSD(T) potential was recently published[18] that gives energy levels that are in semiquantitative agreement with experiment. This surface shows two minima at slipped antipar-

a)Electronic mail: avda@theochem.kun.nl

allel structures: the global minimum with the C–C distance smaller than the O–O distance and a local minimum where the O-atoms are closer together. It was shown that the existence of the two slipped antiparallel structures, occurring at different intermolecular separations, can account for the experimentally observed existence of stacks of rotational levels with different rotational constants.[18]

The supermolecular approach as employed in the CCSD(T) calculations of the CO dimer is certainly the most straightforward and therefore perhaps the most widely used way to extract intermolecular interaction energies from *ab initio* electronic structure calculations. Yet, in the last decade symmetry-adapted intermolecular perturbation theory (SAPT) has emerged as a viable alternative.[19] In SAPT the interaction energy is calculated as a sum of terms of distinct physical origin, i.e., the first-order Coulomb and the second-order induction and dispersion energies, each of these terms being accompanied by a corresponding exchange correction due to the simultaneous exchange of electrons between the monomers. All of these contributions are affected by intramonomer electron correlation. In the many-body version of SAPT (MB-SAPT) (Ref. 20) intramonomer electron correlation is described through Møller-Plesset perturbation theory of various orders, depending on the accuracy requirements for each interaction contribution. In many cases the quality of the total interaction energies is similar to that obtained from CCSD(T) calculations.[21,22]

As an alternative to treating intramonomer electron correlation through many-body perturbation theory it has been proposed to combine SAPT with a relatively inexpensive description of the monomers through density functional theory (DFT).[23,24] Such a combined DFT-SAPT scheme is well founded for the first-order Coulomb and the second-order induction and dispersion energy contributions, which are potentially exact if (time-dependent) coupled-perturbed Kohn–Sham DFT is utilized to calculate the monomer response densities, and provided that the exact exchange-correlation potential (xc-potential) and the exact exchange-correlation kernel (xc-kernel) are known.[24] By contrast, the intermolecular exchange corrections to the first- and second-order contributions are not potentially exact and can only be approximated with DFT-SAPT. Yet, this does not seem to be a serious drawback for practical use of the method: from a comparison of the results of DFT-SAPT with those of MB-SAPT it was found that monomer electron correlation effects on both first-order Coulomb and exchange energies were accurately reproduced, provided that a well-balanced asymptotically correct xc-potential was employed.[25,26] This holds also true for the second-order contributions.[27,28]

The accuracy one can achieve with DFT-SAPT for those cases, where essentially exact xc-potentials can be utilized, has been demonstrated recently for the helium dimer: DFT-SAPT is able to reproduce the best theoretical estimates for the interaction energy within 1% if the effect of third and higher orders of the intermolecular perturbation are estimated on the correlated level.[29] An estimate of the third- and higher-order corrections usually is available on the Hartree-Fock level only. Utilizing the uncorrelated correction the accuracy of DFT-SAPT for the interaction energy of He_2 drops to 5%, but considering the relatively low computational effort of the DFT-SAPT method this is still competitive with CCSD(T), which deviates by 3% from the most reliable estimates.[29]

In this paper, we present a PES for the CO dimer, calculated using DFT-SAPT. We present results of rovibrational calculations on this potential and show that the results are comparable to those of the CCSD(T) potential. Furthermore, we take a step toward creating a quantitatively correct potential, by combining the DFT-SAPT potential and the CCSD(T) potential into a hybrid potential with one empirical parameter. We will show that this hybrid potential gives results that are in very close agreement to the experimental data.

II. DETAILS OF THE CALCULATIONS

A. DFT-SAPT calculations

In the DFT-SAPT calculations the interaction energy was obtained as

$$\Delta E_{\mathrm{AB}} = E_{\mathrm{pol}}^{(1)} + E_{\mathrm{exch}}^{(1)} + E_{\mathrm{ind}}^{(2)} + E_{\mathrm{exch\text{-}ind}}^{(2)} + E_{\mathrm{disp}}^{(2)} + E_{\mathrm{exch\text{-}disp}}^{(2)} + \delta(\mathrm{HF}), \quad (1)$$

where $E_{\mathrm{pol}}^{(1)}$ and $E_{\mathrm{exch}}^{(1)}$ are the first-order Coulomb and exchange interaction energies, $E_{\mathrm{ind}}^{(2)}$ and $E_{\mathrm{exch\text{-}ind}}^{(2)}$ the second-order induction energy and its exchange correction, and $E_{\mathrm{disp}}^{(2)}$ and $E_{\mathrm{exch\text{-}disp}}^{(2)}$ the second-order dispersion energy and its exchange correction, respectively. The last term $\delta(\mathrm{HF})$ is determined from counterpoise-corrected supermolecular Hartree-Fock calculations[20] and describes the effect of third and higher orders in the interaction potential on an uncorrelated level.

All of the intermolecular perturbation contributions up to second order were obtained with a self-written program (attached to the MOLPRO program package[30]) which determines the second-order induction and dispersion energies along with their respective exchange corrections via a coupled (time-dependent) Kohn-Sham DFT approach, as first suggested in Ref. 24. Further methodological details on the calculation of individual interaction energy contributions may be found in Ref. 25 for the first-order terms and Ref. 27 for the second-order induction contributions. As in Ref. 29, the latter were determined from analytical instead of numerical solutions of the coupled-perturbed Kohn-Sham equations. The dispersion energies were calculated from the eigensolutions of the time-dependent DFT equations as described in Ref. 28 (cf. Ref. 31 for an equivalent route to DFT-SAPT dispersion energies) which were also used to determine its exchange correction. The PBE0AC xc-potential, introduced and defined in Ref. 25, was used to determine the Kohn-Sham orbitals, and the xc-kernel employed was of the hybrid adiabatic local density approximation type.[28]

Further technical parameters of the calculations were kept as close as possible to the previous CCSD(T) study of the CO dimer:[18] the Gaussian type function basis set employed consists of the augmented correlation-consistent polarized valence triple zeta aug-cc-pVTZ atomic basis sets[32,33] to which an uncontracted $3s3p2d1f$ set of bond functions

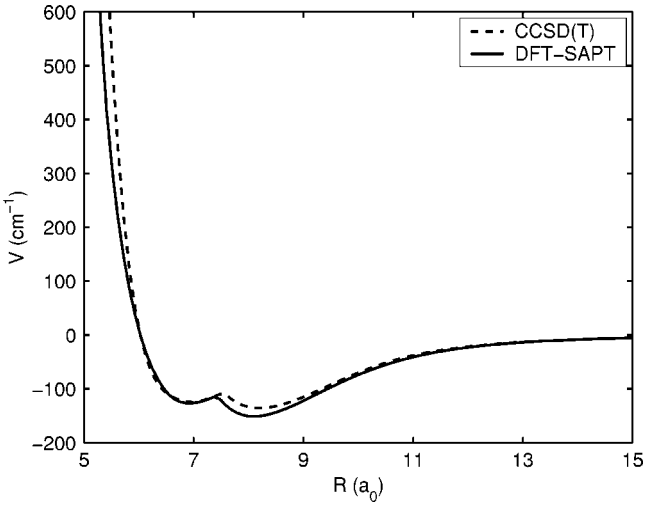

FIG. 1. Comparison of the radial behavior of the DFT-SAPT potential with the CCSD(T) potential of Ref. 18. On each R point, the potential is minimized in the angular coordinates.

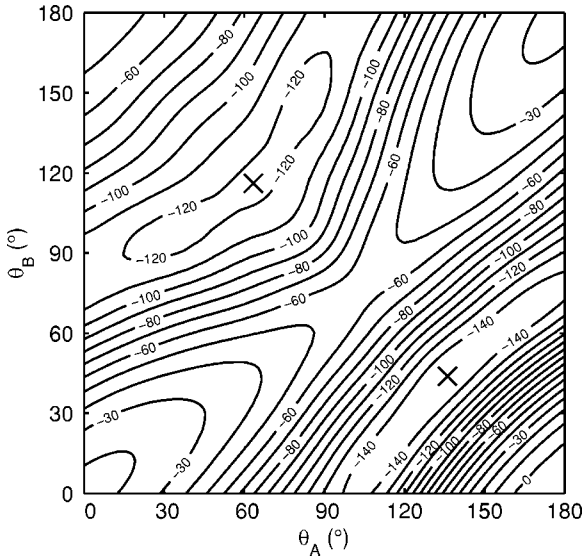

FIG. 2. Cut through the fit of the DFT-SAPT potential for $\phi=180°$. On each (θ_A,θ_B) point the potential is minimized in the R coordinate.

was added at the midpoint between the centers of mass of the CO molecules. The CO bond distance was fixed at 2.132 bohr and the following atom masses were used: 15.994 915 0 u for ^{16}O, 12 u for ^{12}C (by definition), and 13.003 35 48 u for ^{13}C. The interaction energies first were calculated at exactly the same 1512 geometries as discussed in Ref. 18: the angles θ_A and θ_B between the vector $\mathbf{R}$ from the center of mass of monomer A to that of monomer B and the vectors $\mathbf{r}_A$ and $\mathbf{r}_B$ pointing from the C-atom to the O-atom in the monomers, respectively, were varied according to a six-point Gauss-Legendre grid, while the dihedral angle ϕ between the planes defined by $(\mathbf{R},\mathbf{r}_A)$ and $(\mathbf{R},\mathbf{r}_B)$, respectively, was varied according to a six-point Gauss-Chebyshev grid. The distance $R=|\mathbf{R}|$ was varied in steps of 1 bohr for the range 5–10 bohrs, and in steps of 2.5 bohrs for the range between 10 and 25 bohrs. In a second series of calculations these geometries were extended by another 936 geometries, making up for a total of 2448 computed points on the potential energy surface. These points were restricted to the distance range between 5 and 10 bohrs and to the same six values of the dihedral angle ϕ as given above. The θ_A and θ_B grids, however, were refined to include the angles 10°, 62.401 384°, 117.598 616°, and 170°.

B. Analytic fit of the potential

The first step in fitting the potential, was a least squares fit of the calculated interaction energy to angular functions, for each of the 12 intermolecular distances:

$$\Delta E_{AB}(R,\theta_A,\theta_B,\phi) = \sum_{L_A L_B M} C_{L_A L_B M}(R) A_{L_A L_B M}(\theta_A,\theta_B,\phi), \tag{2}$$

with $0\leqslant L_A,L_B\leqslant 6$ and $0\leqslant M\leqslant \min(L_A,L_B,5)$. The angular functions $A_{L_A L_B M}$ are given by

$$A_{L_A L_B M}(\theta_A,\theta_B,\phi)=P_M^{L_A}(\cos\theta_A)P_M^{L_B}(\cos\theta_B)\cos M\phi, \tag{3}$$

where the $P_M^{L_X}$ are Schmidt seminormalized associated Legendre functions. The resulting expansion coefficients were then subjected to a similar fit procedure as used in the fit of CCSD(T) potential.[18] First the long-range part was fitted as in the earlier work

$$C_{L_A L_B M}(R)=c_{L_A L_B M}/R^{\nu_{L_A L_B M}} \quad \text{for} \quad R\geqslant 15a_0. \tag{4}$$

It was verified that the numbers $\nu_{L_A L_B M}$ are close to what is predicted by long-range theory. For instance, the contributions with $(L_A L_B M)=(2\,2\,0)$, $(2\,2\,1)$, and $(2\,2\,2)$ constitute (together with a Clebsch-Gordan coupling coefficient) the important quadrupole-quadrupole interaction. The exponents $\nu_{2\,2\,M}$ are, respectively, 4.92, 4.96, and 4.97, while in the multipole expansion they are 5 exactly. We also experimented with the usual long-range terms that have the exact integer exponents, but it turned out that the form chosen is easy to fit and needs fewer parameters, while giving a better fit of the expansion coefficients over a wide range of distances. Certain $(L_A L_B M)$ combinations do not appear in the long range, in those cases $c_{L_A L_B M}$ was put equal to zero.

These long-range terms were damped with a Tang-Toennies[34] damping function $T(R;n_{L_A L_B M},\alpha_{L_A L_B M})$ and subtracted from the original coefficients to give the short-range coefficients:

TABLE I. Well depths and equilibrium geometries of the DFT-SAPT and CCSD(T) potentials. The dihedral angle ϕ equals 180°.

	R_e (bohrs)	θ_A	θ_B	D_e (cm^{-1})
	DFT-SAPT potential			
Global minimum	8.15	136.1	43.9	−148.37
Local minimum	6.92	63.6	116.4	−121.77
	CCSD(T) potential[a]			
Global minimum	8.20	134.2	45.8	−135.53
Local minimum	6.95	59.6	120.4	−124.21

[a]Reference 18.

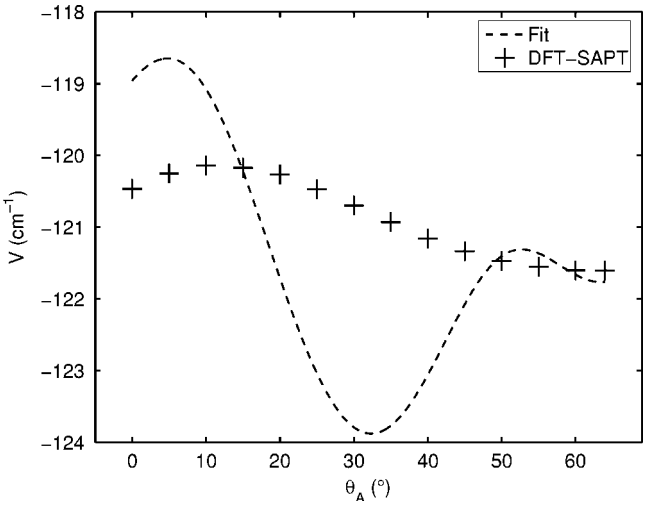

FIG. 3. Comparison of calculated DFT-SAPT points and fitted potential, for $\phi=180°$. For each θ_A point, the potential is minimized with respect to R and θ_B. The minimum around $\theta_A=32°$ is due to errors in the fit.

$$C^{\mathrm{SR}}_{L_AL_BM}(R)=C_{L_AL_BM}(R) - T(R;n_{L_AL_BM},\alpha_{L_AL_BM})c_{L_AL_BM}/R^{\nu_{L_AL_BM}}. \tag{5}$$

The short-range terms were then finally fitted to the form

$$C^{\mathrm{SR}}_{L_AL_BM}(R)=\exp(-\alpha_{L_AL_BM}R)\sum_{k=0}^{4} d_{L_AL_BM}R^k. \tag{6}$$

The integers $n_{L_AL_BM}$ used in the Tang-Toennies damping function were taken to be the integer nearest to $\nu_{L_AL_BM}$. The $\alpha_{L_AL_BM}$ that appear both in the damping function and the short-range fitting functions were obtained by starting with all α's equal to unity and iterating the fitting procedure until they converged.

C. Rovibrational calculations

The methodology for computing the rovibrational bound states of the dimer is the same as was used previously in Ref. 18. Since in the rovibrational calculations the Wigner-Eckart theorem is applied, it was more convenient to have the potential expanded in coupled angular functions. Therefore the fitted potential was first reexpanded in functions

TABLE II. Calculated values characterizing rotational stacks for ^{12}CO dimer, from the DFT-SAPT potential energy surface. The effective intermolecular distance $R_{\mathrm{eff}}=(2\mu B)^{-1/2}$.

Stack	K	Symmetry	R_{eff}	Origin (cm^{-1})	B (cm^{-1})	D (cm^{-1})
a	0	A^+	$8.49a_0$	0.00	0.059 67	1.6×10^{-6}
b	1	A^+	$8.40a_0$	2.39	0.060 89	4.2×10^{-5}
c	0	A^+	$7.52a_0$	6.31	0.075 98	5.5×10^{-6}
d	1	A^+	$7.36a_0$	8.44	0.079 31	1.0×10^{-4}
e	0	A^-	$8.46a_0$	4.89	0.060 03	1.8×10^{-6}
f	1	A^-	$7.64a_0$	11.03	0.073 73	4.4×10^{-5}
g	1	A^+	$7.94a_0$	11.59	0.068 14	8.6×10^{-5}
j	0	A^-	$7.89a_0$	9.95	0.069 10	-3.2×10^{-6}
k	1	A^-	$8.47a_0$	6.46	0.059 90	-2.3×10^{-5}

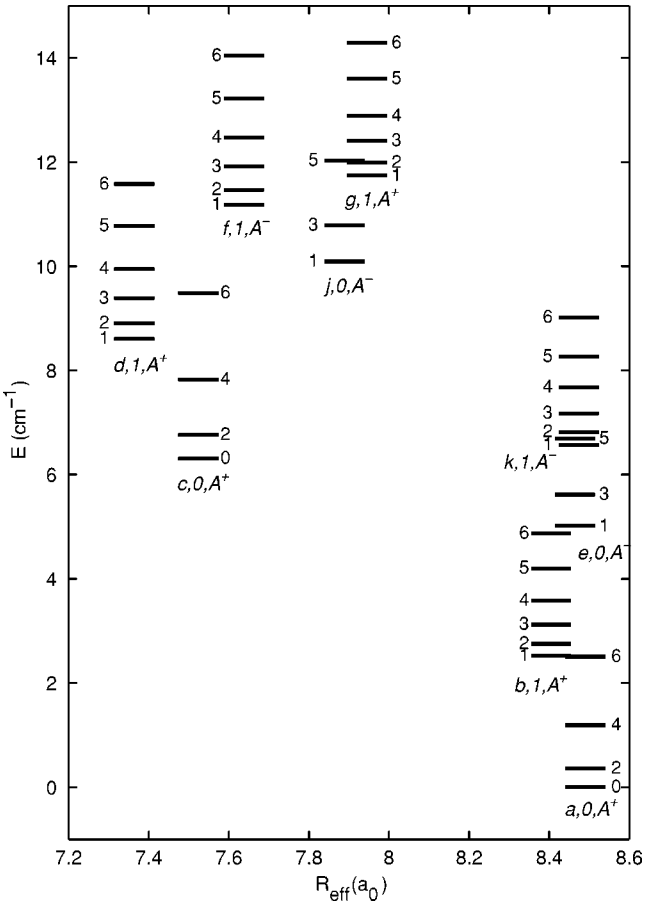

FIG. 4. Computed stacks of rotational levels of ^{12}CO dimer on the DFT-SAPT potential, plotted against $R_{\mathrm{eff}}=(2\mu B)^{-1/2}$, where the rotational constant B was determined by fitting a rigid rotor expression to the computed energy levels.

$$A_{L_AL_BL}(\theta_A,\theta_B,\phi)=\sum_{M=0}^{\min(L_A,L_B)}(-1)^M\begin{pmatrix} L_A & L_B & L \\ M & -M & 0\end{pmatrix} \times P_M^{L_A}(\cos\theta_A)P_M^{L_B}(\cos\theta_B)\cos M\phi \tag{7}$$

for each point on the radial grid, consisting of 243 equally spaced points in the range $5a_0-30a_0$.

The Hamiltonian was represented in a direct product basis of radial and angular basis functions:

$$|n(j_Aj_B)j_{AB}K;JM\rangle=|n\rangle|(j_Aj_B)j_{AB}K;JM\rangle. \tag{8}$$

The angular basis functions are defined in Ref. 18. The radial functions are $|n\rangle\equiv\chi_n(R)/R$, where the χ_n are eigenfunctions of a reference Hamiltonian

$$H^{\mathrm{ref}}=-\frac{1}{2\mu_{AB}}\frac{\partial^2}{\partial R^2}+V^{\mathrm{ref}}. \tag{9}$$

Here, μ_{AB} denotes the reduced mass of the dimer and V^{ref} is a reference potential. The basis functions χ_n were computed with a sinc function discrete variable representation on the radial grid. The reference potential was obtained by first minimizing the full PES in the angular coordinates on each grid point in R, after which a Morse potential

$$V^{\mathrm{M}}(R)=D_{\mathrm{M}}\{1-\exp[-a_{\mathrm{M}}(R-R_0)]\}^2 \tag{10}$$

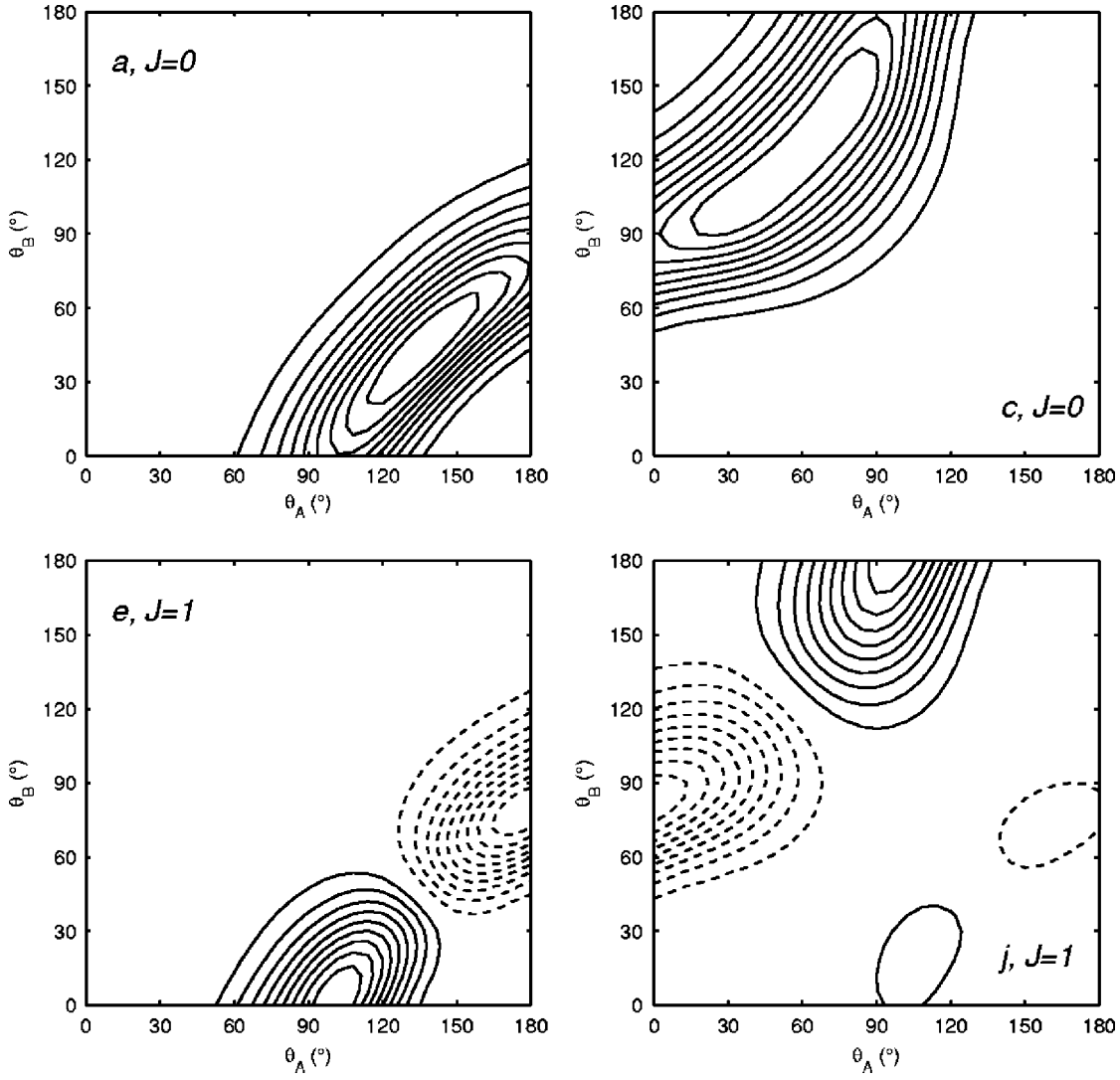

FIG. 5. Cuts through the wave function of the lowest level in the $K=0$ stacks on the DFT-SAPT potential: $(a,J=0)$ (upper left), $(c,J=0)$ (upper right), $(e,J=1)$ (lower left), and $(j,J=1)$ (lower right). The cuts are for $\phi=180°$ and $R=R_{\mathrm{eff}}$. Contours are drawn at values $\pm k|\psi|_{\max}/10$ for $k=1,...,9$.

was fitted through a physically meaningful subset of the resulting values. This procedure gave $D_{\mathrm{M}}=247.79\ \mathrm{cm}^{-1}$, $a_{\mathrm{M}}=0.6200a_0^{-1}$, and $R_0=7.0129a_0$. To obtain a basis in which also the effect of the continuum on the wave function could be represented, the Morse potential was extrapolated linearly for $R>10.05a_0$, leading to V^{ref}.

The first 15 radial basis function and angular functions up to $j_A, j_B=10$ were used in the calculations. Rovibrational states were calculated for total angular momentum up to and including $J=6$, both for ^{12}CO dimer and the isotopically substituted ^{13}CO dimer. Off-diagonal Coriolis terms, coupling blocks with different K values, were taken into account. The monomer rotational constants were fixed at $1.9317\ \mathrm{cm}^{-1}$ for ^{12}CO and $1.8465\ \mathrm{cm}^{-1}$ for ^{13}CO, consistent with the monomer bond length of $2.132a_0$. Since ^{12}CO is of nuclear spin zero, only states with A^+ or A^- symmetry are allowed for the ^{12}CO dimer. The ^{13}C nucleus has a spin of 1/2, however, so this restriction does not apply to this isotopomer, and levels for all four symmetries $(A^{\pm},B^{\pm})$ were calculated.

When substituting ^{12}C by ^{13}C, the centers of mass in the

TABLE III. Calculated values characterizing rotational stacks for ^{13}CO dimer, from the DFT-SAPT potential energy surface. In the symmetry column, the first label refers to the symmetry of the even J levels in the stack, and the second to that of the odd J states. For the f stacks, also a fit with only the lowest three J states $(J=1,2,3)$ is shown.

Stack	K	Symmetry	R_{eff}	Origin (cm^{-1})	B (cm^{-1})	D (cm^{-1})
a	0	A^+/B^-	$8.44a_0$	0.00	0.058 22	1.4×10^{-6}
b_1	1	B^-/A^+	$8.50a_0$	2.26	0.057 48	0.9×10^{-6}
b_2	1	A^+/B^-	$8.41a_0$	2.26	0.058 70	1.3×10^{-6}
c	0	A^+/B^-	$7.57a_0$	6.95	0.072 51	5.7×10^{-6}
d_1	1	B^-/A^+	$7.64a_0$	9.03	0.071 08	9.6×10^{-6}
d_2	1	A^+/B^-	$7.50a_0$	9.03	0.073 82	7.4×10^{-6}
e	0	B^+/A^-	$8.43a_0$	4.83	0.058 37	1.5×10^{-6}
f_1	1	A^-/B^+	$8.27a_0$	11.41	0.060 65	-2.4×10^{-4}
f_1[a]			$7.72a_0$	11.37	0.069 60	5.1×10^{-5}
f_2	1	B^+/A^-	$8.34a_0$	11.41	0.059 73	-2.5×10^{-4}
f_2[a]			$7.78a_0$	11.37	0.068 61	3.9×10^{-5}
g_1	1	B^-/A^+	$8.20a_0$	11.54	0.061 71	-1.0×10^{-6}
g_2	1	A^+/B^-	$8.05a_0$	11.54	0.064 11	2.1×10^{-6}
j	0	B^+/A^-	$7.90a_0$	10.29	0.066 49	-2.1×10^{-6}
k_1	1	A^-/B^+	$8.42a_0$	6.36	0.058 57	2.4×10^{-6}
k_2	1	B^+/A^-	$8.36a_0$	6.36	0.059 37	2.6×10^{-6}

[a]Fit with $J\leqslant3$ states only.

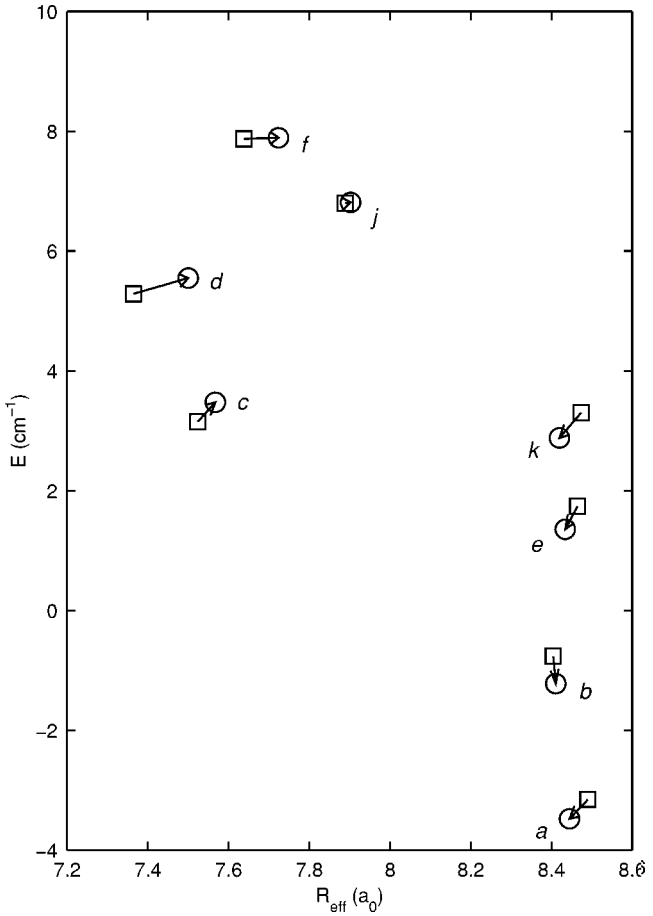

FIG. 6. Isotopic shifts of the stack origins for the CO dimer on the DFT-SAPT potential. The squares represent the origins of $(^{12}CO)_2$, and the circles those of $(^{13}CO)_2$. The zero point of energy is chosen halfway between the *a* and *c* origins, for both isotopes.

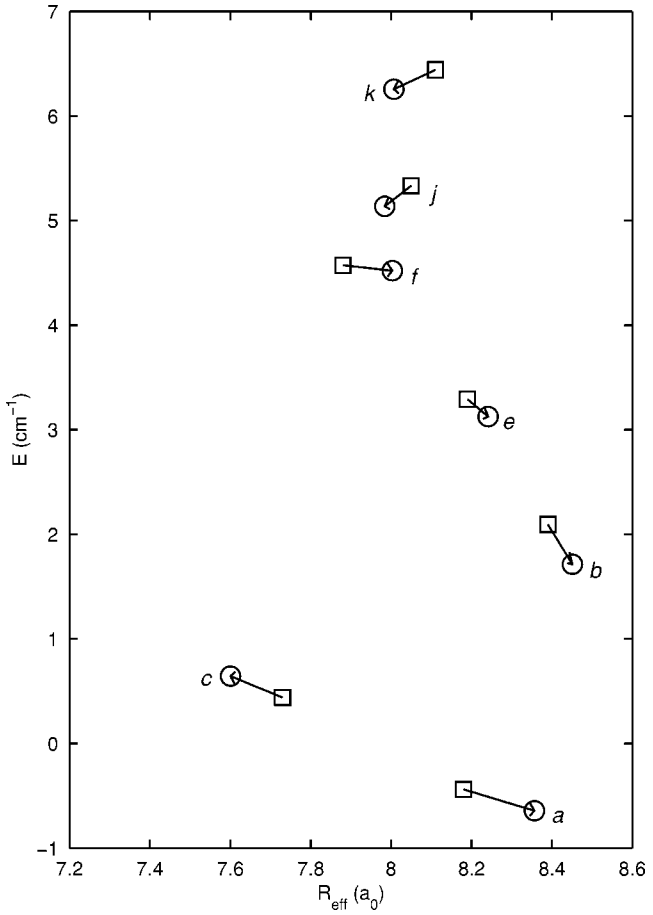

FIG. 7. Experimental isotopic shifts of the stack origins for the CO dimer (reproduced from Fig. 1 in Ref. 13).

CO molecules shift slightly. To account for this effect, the coordinates R, θ_A, θ_B, and ϕ for ^{13}CO dimer were transformed to coordinates describing the same geometry in ^{12}CO dimer using the formulas from Ref. 35, and the potential was again reexpanded, this time using angular functions up to $L_A, L_B = 7$ inclusive.

III. RESULTS

A. DFT-SAPT potential

In Fig. 1, the radial dependence of the DFT-SAPT potential is compared to that of the previous CCSD(T) potential.[18] On each point on the R grid, the potential is minimized in all three angular coordinates. The DFT-SAPT potential shows the same double-well structure as the CCSD(T) potential; the difference in energy between the global minimum (at larger R) and the local minimum (at smaller R) is more pronounced in the DFT-SAPT surface. Furthermore, the global minimum is located at a slightly shorter intermolecular distance than for the CCSD(T) potential.

The angular dependence of the DFT-SAPT potential is shown in Fig. 2. The figure is a cut through the full surface, for $\phi = 180°$, and R values that minimize the potential in each (θ_A, θ_B) point. Overall, the shape is the same as that of the CCSD(T) potential. The depths of the two wells in both potentials and the corresponding geometries are compared in Table I. Due to the truncation of the expansion in Eq. (2) to $L_A, L_B \leqslant 6$, the fit contains small errors, especially in the valley around the local minimum. In Fig. 3, the potential along a minimum energy path through this valley is shown. It shows that the points calculated with the DFT-SAPT method smoothly go down to a minimum on the $\theta_A = \pi - \theta_B$ diagonal, and that the fit oscillates around these points. The oscillations are strong enough to cause a shallow (≈ 2 cm^{-1}), unphysical minimum away from the $\theta_A = \pi - \theta_B$ axis around $\theta_A = 32°$. The largest absolute error in the bound ($V < 0$) regions of the potential is 6.4 cm^{-1}, with an average error of 0.17 cm^{-1}. The largest relative error in the repulsive part of

TABLE IV. Calculated values characterizing rotational stacks for ^{12}CO dimer, from the hybrid potential energy surface.

Stack	K	Symmetry	R_{eff}	Origin (cm^{-1})	B (cm^{-1})	D (cm^{-1})
a	0	A^+	$8.21a_0$	0.00	0.063 83	4.1×10^{-5}
b	1	A^+	$8.32a_0$	2.50	0.062 16	5.7×10^{-5}
c	0	A^+	$7.76a_0$	0.89	0.071 37	-3.4×10^{-5}
d	1	A^+	$7.45a_0$	2.66	0.077 51	6.1×10^{-5}
e	0	A^-	$8.15a_0$	3.54	0.064 77	1.1×10^{-5}
f	1	A^-	$8.04a_0$	5.13	0.066 52	-1.2×10^{-5}
g	1	A^+	$7.88a_0$	8.26	0.069 23	5.9×10^{-5}
j	0	A^-	$8.15a_0$	5.75	0.064 80	-1.8×10^{-5}
k	1	A^-	$8.12a_0$	6.99	0.065 28	-3.0×10^{-6}

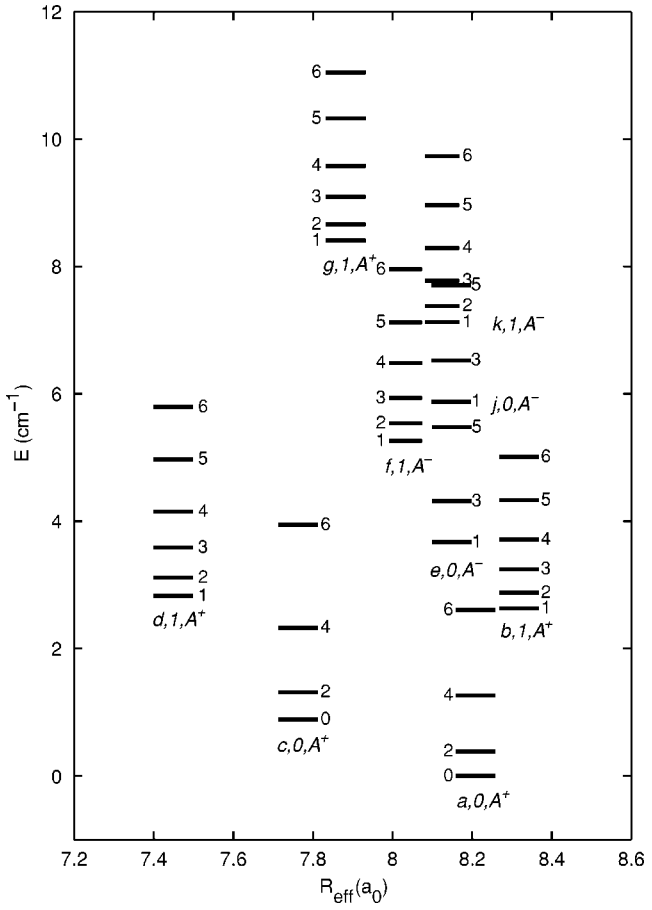

FIG. 8. As Fig. 4, for the hybrid potential.

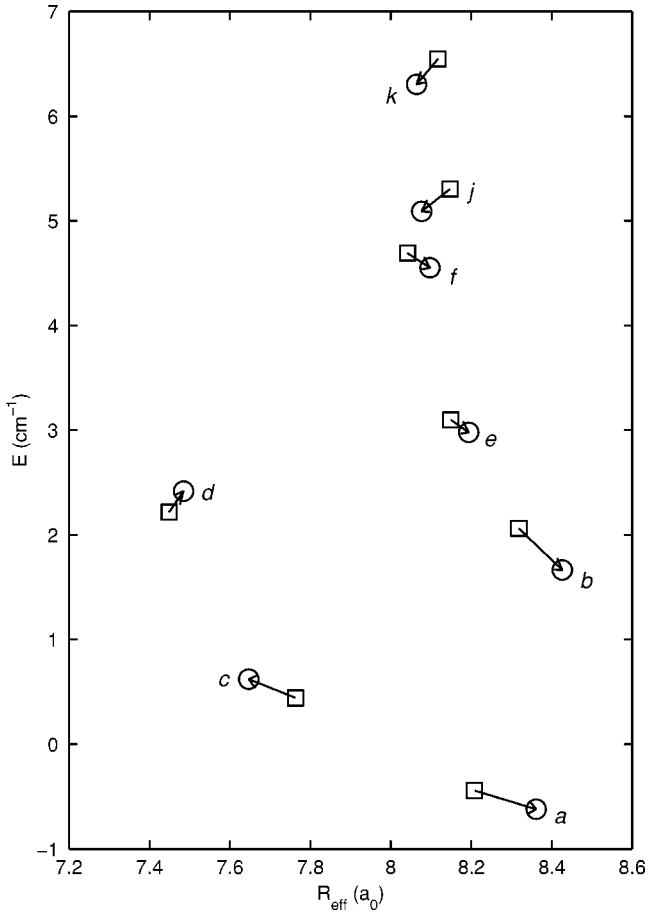

FIG. 9. As Fig. 6, for the hybrid potential.

the potential ($V>150$ cm^{-1}) is $\approx 10\%$, with an average error of 1.8%. Although these errors may seem relatively large, they must be put in context. In the first place, the difference between the DFT-SAPT potential and the CCSD(T) potential is substantially larger than the fit errors. Since we will finally use a weighted average of the two potentials, it does not pay to spend much more attention on improving the fit. Second, the dominant source of the error shown in Fig. 3 is the truncation of the expansion in Eq. (2) to $L_A, L_B \leqslant 6$. Extension of this expansion would require many more CCSD(T) and DFT-SAPT calculations, while the calculated rovibrational levels are rather insensitive to the small oscillations in the potential caused by the truncation of the expansion.

TABLE V. Calculated values characterizing rotational stacks for ^{13}CO dimer, from the hybrid potential energy surface.

Stack	K	Symmetry	R_{eff}	Origin (cm^{-1})	B (cm^{-1})	D (cm^{-1})
a	0	A^+/B^-	$8.36a_0$	0.00	0.059 393	1.3×10^{-5}
b_1	1	B^-/A^+	$8.50a_0$	2.29	0.057 482	-7.4×10^{-6}
b_2	1	A^+/B^-	$8.43a_0$	2.29	0.058 482	3.0×10^{-6}
c	0	A^+/B^-	$7.65a_0$	1.24	0.071 007	2.8×10^{-6}
d_1	1	B^-/A^+	$7.61a_0$	3.04	0.071 653	1.3×10^{-6}
d_2	1	A^+/B^-	$7.48a_0$	3.04	0.074 113	2.1×10^{-6}
e	0	B^+/A^-	$8.19a_0$	3.60	0.061 847	9.3×10^{-6}
f_1	1	A^-/B^+	$8.10a_0$	5.17	0.063 331	2.4×10^{-5}
f_2	1	B^+/A^-	$8.01a_0$	5.17	0.064 647	2.0×10^{-5}
g_1	1	B^-/A^+	$8.29a_0$	8.22	0.060 411	-1.7×10^{-4}
[a]			$8.15a_0$	8.22	0.062 490	-4.7×10^{-5}
g_2	1	A^+/B^-	$8.08a_0$	8.22	0.063 519	-1.1×10^{-4}
[a]			$7.96a_0$	8.22	0.065 519	-1.3×10^{-5}
j	0	B^+/A^-	$8.08a_0$	5.71	0.063 653	-9.1×10^{-6}
k_1	1	A^-/B^+	$8.06a_0$	6.93	0.063 853	-1.4×10^{-5}
k_2	1	B^+/A^-	$8.09a_0$	6.93	0.063 365	-1.7×10^{-5}

[a]Fit with $J\leqslant 3$ states only.

Rovibrational states were calculated on this potential, and, as was the case for the CCSD(T) potential, we were able to organize these levels in different stacks of different rotational constants. Each stack was fitted separately using a simple rigid rotor expression

$$E = E_0 + BJ(J+1) - DJ^2(J+1)^2, \tag{11}$$

and the resulting parameters are summarized in Table II. In the labeling of the stacks, the experimental assignments are followed.[7–12,14] Figure 4 shows the calculated stacks as a function of their effective intermolecular distance $R_{\text{eff}} = (2\mu B)^{-1/2}$.

In Fig. 5 cuts through the wave functions of the $K=0$ stacks are drawn. For each stack, the cut is made for $\phi = 180°$, and $R = R_{\text{eff}}$ of that stack. It can be seen that the a stack wave function corresponds to the isomer with the C–C distance smaller than the O–O distance. The wave functions in the c stack correspond to the other isomer with the shorter O–O distance. The e and j wave functions clearly show excitations of the geared bending motions of the two isomers. The very low excitation frequency of ≈ 4 cm^{-1} indi-

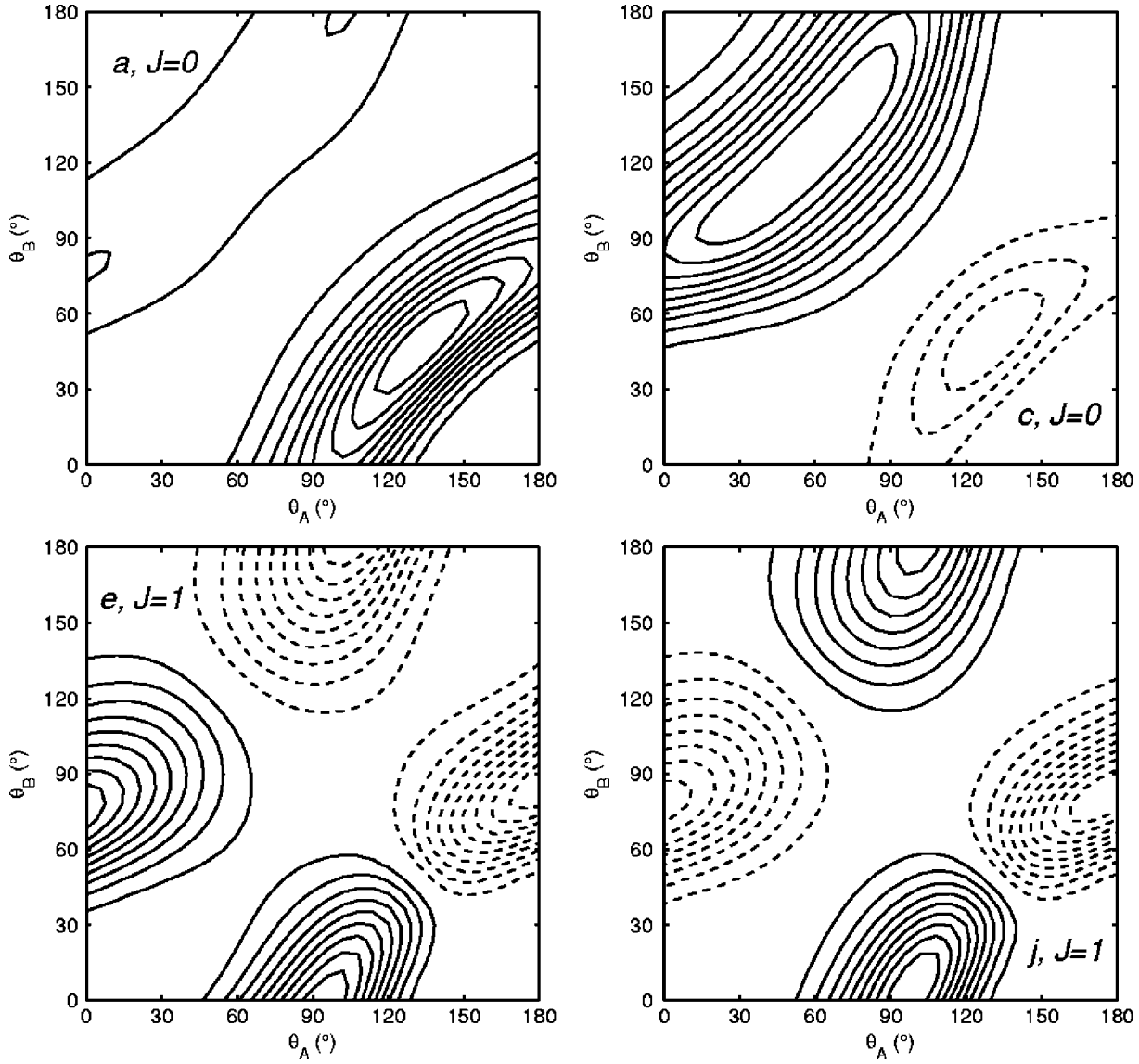

FIG. 10. As Fig. 5, for the hybrid potential.

cates that the dimer is indeed very floppy. Since the artificial minima in the fit of the potential are very shallow ($\approx 2\ \mathrm{cm}^{-1}$), the effect on the dynamics of the dimer is negligible. Inspection of the wave functions shows no effect of these minima on the wave functions that are located in the valley around them, i.e., those corresponding to the *c* and *j* stacks.

Recently, a substantial amount of experimental data on the isotopically substituted ^{13}CO dimer has become available.[13,14] To test the potential surface, we also calculated the rovibrational levels of $(^{13}\mathrm{CO})_2$. Since the total nuclear spin of ^{13}CO is not zero, also levels of $B^{\pm}$ symmetry exist for this dimer. This results in the $K=0$ stacks having both even and odd J levels, and the $K=1$ stacks splitting up in two separate stacks: one where the even J levels are of $A^{\pm}$ symmetry and the odd J levels are of $B^{\mp}$ symmetry, and one where the situation is reversed. The resulting data are collected in Table III. For the *f* states, significant Coriolis mixing with $K=2$ states occurred for the rotational levels $J \geqslant 4$. This greatly influenced the rotational constants, as can be seen in Table III. Since the DFT-SAPT potential is not sufficiently accurate to predict these couplings well, these stacks were also fitted with the $J \leqslant 3$ levels only.

Following the experimental papers, we have drawn in Fig. 6 the isotope shifts of the stack origins. For both isotopomers, the energy zero is chosen halfway between the *a* and *c* stack origins. Comparing this picture with the experimental figure in Ref. 13, reproduced here as Fig. 7, it can be seen that the agreement with experiment is very bad. Nearly all R_{eff} values shift in the wrong direction, and the differences are much smaller than those in the experiment. The results on the DFT-SAPT surface suggest a nearly static isotope effect where the change in rotational constants is mainly due to the shift of the centers of mass in the monomers and the average geometry of the complex is not changed. They cannot account for the opposite and much stronger effect that was found experimentally.

Calculations on $(^{13}\mathrm{CO})_2$ on the CCSD(T) potential show that it does not predict the isotope effect any better than the DFT-SAPT potential. Also on the CCSD(T) potential, the

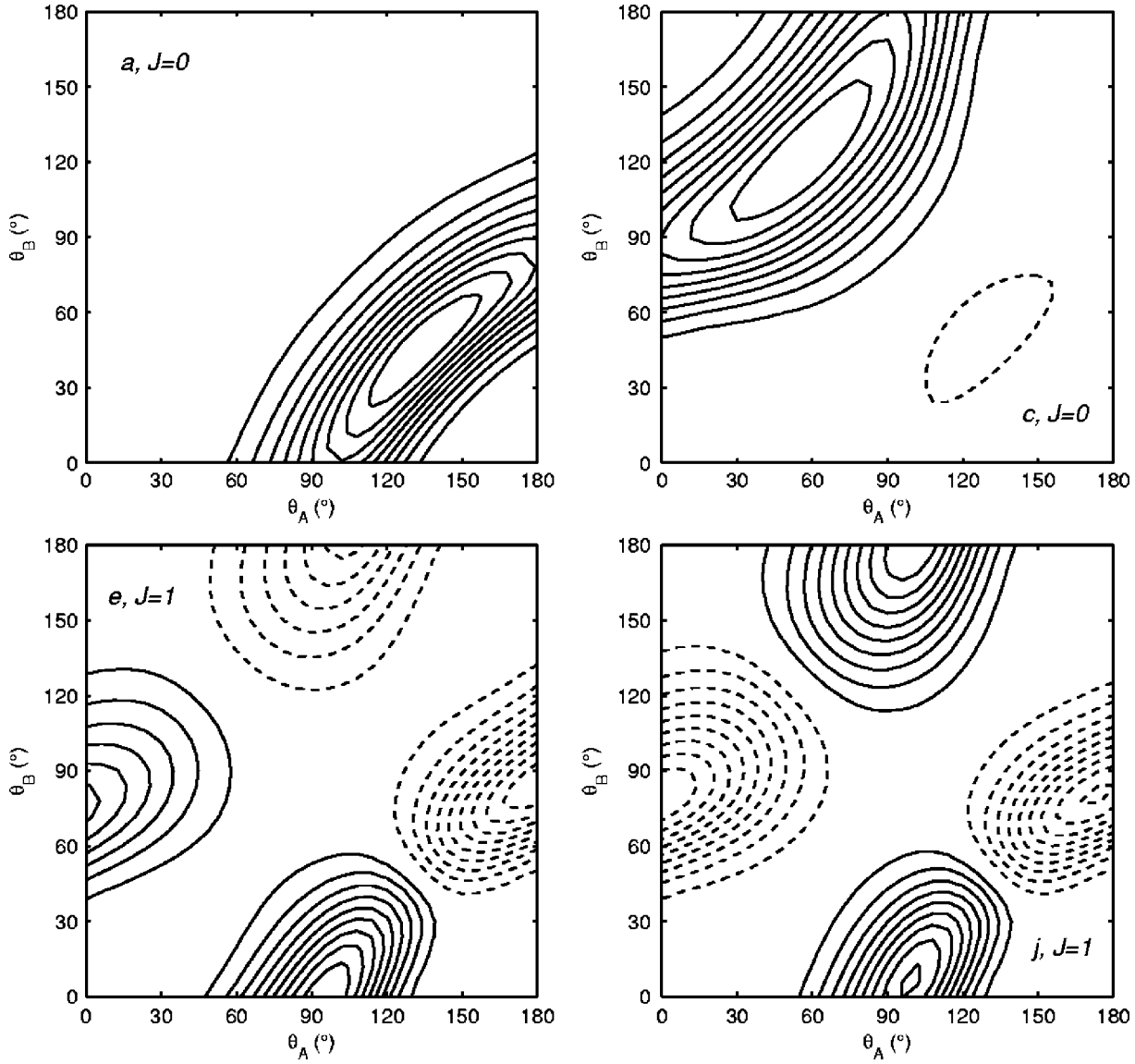

FIG. 11. As Fig. 5, for $(^{13}CO)_2$ on the hybrid potential.

R_{eff} values of the stack origins shift only very little, and in the wrong direction.

B. Tuning: A hybrid potential

When comparing the calculated rotational stacks that result from the DFT-SAPT potential with those from CCSD(T) potential, the first thing one notices is that the order of the origins of *a* and *c* stacks is reversed. Although also in the CCSD(T) potential the global minimum is located around $\theta_A=135°, \theta_B=45°$, the zero point energy in this minimum is so large that it overcomes the difference of $\approx 11\ \mathrm{cm}^{-1}$ with the local minimum.[18] The difference in zero point energy between the two minima is due to the fact that the well at the global minimum is much narrower than at the local minimum. The DFT-SAPT potential gives the correct sign for the energy difference between the *a* and *c* stack origins, however, it overestimates the value of this difference. In an attempt to obtain a potential that gives better quantitative information, we constructed a hybrid energy surface as a weighted average of the two potentials,

$$V^{\mathrm{hybrid}} = wV^{\mathrm{CCSD(T)}} + (1-w)V^{\mathrm{DFT\text{-}SAPT}}, \tag{12}$$

where the weighting coefficient w was chosen in such a way that the experimental value for the energy difference $\Delta E = E(c,J=0) - E(a,J=0)$ was reproduced. The resulting value for this weighting coefficient was $w=0.7$.

The calculated rovibrational energy levels from this hybrid potential for ^{12}CO dimer are given in Table IV and a pictorial representation is shown in Fig. 8. One can see that the adjustment of the potential to reproduce the splitting between the *a* and *c* stacks has a positive effect on the other stacks as well. The experimentally determined stack origins are reproduced very well, the maximum error being $0.25\ \mathrm{cm}^{-1}$. Also the computed rotational constants agree better with their experimental counterparts for most stacks.

Rovibrational levels for the isotopically substituted ^{13}CO dimer were also calculated on the hybrid potential, and the results are summarized in Table V. This time the g stacks are very strongly mixed with $K=2$ states for $J \geqslant 4$. Also for the heavier isotope, the hybrid potential gives results that are much closer to the experimental data. Comparing Fig. 9 with the experimental picture in Fig. 7 shows that not only do the isotope shifts have the correct sign on the hybrid potential, also the magnitude of the shifts is in much better agreement with the experimental data. Unfortunately, the g stack has not been observed for $(^{13}CO)_2$, leaving us without a check of whether the strong Coriolis coupling that the hybrid potential predicts for these stacks is real.

It is obvious from Figs. 6 and 9 that the isotopic shifts are very sensitive to the exact shape of the potential. Since the overall shape of the CCSD(T) and DFT-SAPT potentials is more or less the same, taking a linear combination of these two corresponds roughly to shifting the two deepest minima with respect to each other. Although the change in the difference between the two wells is only a few wave numbers [from $\approx 26.5\ \mathrm{cm}^{-1}$ on the DFT-SAPT surface and $\approx 11\ \mathrm{cm}^{-1}$ on the CCSD(T) surface, to $\approx 15.5\ \mathrm{cm}^{-1}$ on the hybrid surface], the effect on the isotopic dependence of the system is large. The reason for that can be seen when we compare the wave functions for $(^{12}CO)_2$ on both surfaces. Figures 5 and 10 show cuts through the lowest $K=0$ wave functions from the DFT-SAPT and the hybrid PES, respectively. The cuts are for $\phi = 180°$ and $R = R_{\mathrm{eff}}$. We see that on the hybrid surface, the wave functions are much more delocalized than on the DFT-SAPT surface. Whereas the wave functions on the DFT-SAPT potential are located in either of the two wells, with little or no density in the other well, the wave functions on the hybrid surface are delocalized over both wells. This reduces the difference between the wave functions of the a/e and c/j stacks, with the result that the resulting R_{eff} values (which are different for the two wells) are also more alike. For the ^{13}CO dimer, this effect is much smaller (see Fig. 11), since the wave functions are better localized in the two wells due to the heavier mass of the molecules. Hence, the observed behavior of the isotope effect is of a truly dynamical nature, and can only be described correctly if the relative depth of the minima is such that the wave function can tunnel through the barrier between them.

IV. CONCLUSION

The DFT-SAPT method was employed to compute a four-dimensional PES for the CO dimer. The overall shape of the potential is the same as that of a previously published CCSD(T) potential. As in the experiment, stacks of rovibrational levels could be identified and assigned in the calculated results. Though the agreement between calculations and experiment is not yet perfect, the rovibrational calculations show that the DFT-SAPT and the CCSD(T) surfaces are of comparable quality, making DFT-SAPT a viable alternative for the vastly more expensive CCSD(T) method.

In an effort to overcome the deficiencies of the two *ab initio* potentials, a hybrid potential was constructed by taking a weighted average of the DFT-SAPT and the CCSD(T) potential. The weighting factor was optimized only to reproduce the energy splitting between the two lowest $J=0$ levels, but the resulting surface proved to give a huge improvement on the location of all observed stacks.

Neither the CCSD(T) nor the DFT-SAPT potential alone can explain the observed differences in the effective intermolecular separation R_{eff} between $(^{12}CO)_2$ and $(^{13}CO)_2$. This is mainly due to the fact that the R_{eff} values for the ^{12}CO dimer are very sensitive to the relative location of the two deepest minima in the potential. The hybrid potential gives shifts that are in good agreement with the experimental values.

ACKNOWLEDGMENTS

The authors wish to thank Professor G. Winnewisser for encouraging them to study the CO dimer. Also, they thank Professor Winnewisser and Dr. A. R. W. McKellar for sharing their results prior to publication. A.H. and G.J. are grateful for financial support of this work through the Deutsche Forschungsgemeinschaft (DFG). G.W.M.V. gratefully acknowledges financial support of the Council for Chemical Sciences of the Netherlands Organization for Scientific Research (CW-NWO).

[1] P. A. Vanden Bout, J. M. Steed, L. S. Bernstein, and W. Klemperer, Astrophys. J. **234**, 503 (1979).
[2] M. Havenith, M. Petri, C. Lubina, G. Hilpert, and W. Urban, J. Mol. Spectrosc. **167**, 248 (1994).
[3] M. D. Brookes and A. R. W. McKellar, Chem. Phys. Lett. **287**, 365 (1998).
[4] M. Rode, J. Sadlej, R. Moszynski, P. E. S. Wormer, and A. van der Avoird, Chem. Phys. Lett. **314**, 326 (1999).
[5] T. B. Pedersen, B. Fernández, and H. Koch, Chem. Phys. Lett. **334**, 419 (2001).
[6] M. Rode, J. Sadlej, R. Moszynski, P. E. S. Wormer, and A. van der Avoird, Chem. Phys. Lett. **334**, 424 (2001).
[7] M. D. Brookes and A. R. W. McKellar, J. Chem. Phys. **111**, 7321 (1999).
[8] D. A. Roth, M. Hepp, I. Pak, and G. Winnewisser, Chem. Phys. Lett. **298**, 381 (1998).
[9] D. A. Roth, L. A. Surin, B. S. Dumesh, G. Winnewisser, and I. Pak, J. Chem. Phys. **113**, 3034 (2000).
[10] K. A. Walker, C. Xia, and A. R. W. McKellar, J. Chem. Phys. **113**, 6618 (2000).
[11] K. A. Walker and A. R. W. McKellar, J. Mol. Spectrosc. **208**, 209 (2001).
[12] J. Tang, A. R. W. McKellar, L. A. Surin, D. N. Fourzikov, B. S. Dumesh, and G. Winnewisser, J. Mol. Spectrosc. **214**, 87 (2002).
[13] L. A. Surin, D. N. Fourzikov, B. S. Dumesh, G. Winnewisser, J. Tang, and A. R. W. McKellar, J. Mol. Spectrosc. **223**, 132 (2004).
[14] A. R. W. McKellar, J. Chem. Phys. **115**, 3571 (2001).
[15] A. van der Pol, A. van der Avoird, and P. E. S. Wormer, J. Chem. Phys. **92**, 7498 (1990).
[16] A. W. Meredith and A. J. Stone, J. Phys. Chem. A **102**, 434 (1998).
[17] P. R. Bunker, P. Jensen, S. C. Althorpe, and D. C. Clary, J. Mol. Spectrosc. **157**, 208 (1993).
[18] G. W. M. Vissers, P. E. S. Wormer, and A. van der Avoird, Phys. Chem. Chem. Phys. **5**, 4767 (2003).
[19] B. Jeziorski, R. Moszynski, and K. Szalewicz, Chem. Rev. (Washington, D.C.) **94**, 1887 (1994).
[20] B. Jeziorski, R. Moszynski, A. Ratkiewicz, S. Rybak, K. Szalewicz, and H. L. Williams, *Methods and Techniques in Computational Chemistry: METECC-94*, Medium Size Systems Vol. B (STEF, Cagliari, 1993), pp. 79–129.
[21] G. C. McBane and S. M. Cybulski, J. Chem. Phys. **110**, 11734 (1999).
[22] A. J. Misquitta, R. Bukowski, and K. Szalewicz, J. Chem. Phys. **112**, 5308 (2000).
[23] H. L. Williams and C. F. Chabalowski, J. Phys. Chem. A **105**, 646 (2001).
[24] G. Jansen and A. Heßelmann, J. Phys. Chem. A **105**, 11156 (2001).
[25] A. Heßelmann and G. Jansen, Chem. Phys. Lett. **357**, 464 (2002).
[26] A. J. Misquitta and K. Szalewicz, Chem. Phys. Lett. **357**, 301 (2002).
[27] A. Heßelmann and G. Jansen, Chem. Phys. Lett. **362**, 319 (2002).

[28] A. Heßelmann and G. Jansen, Chem. Phys. Lett. **367**, 778 (2003).
[29] A. Heßelmann and G. Jansen, Phys. Chem. Chem. Phys. **5**, 5010 (2003).
[30] H.-J. Werner, P. J. Knowles, M. Schütz, *et al.* MOLPRO, version 2002.6, a package of *ab initio* programs.
[31] A. J. Misquitta, B. Jeziorski, and K. Szalewicz, Phys. Rev. Lett. **91**, 033201 (2003).
[32] T. H. Dunning, J. Chem. Phys. **90**, 1007 (1989).
[33] R. A. Kendall, T. H. Dunning, and R. J. Harrison, J. Chem. Phys. **96**, 6796 (1992).
[34] K. T. Tang and J. P. Toennies, J. Chem. Phys. **80**, 3726 (1984).
[35] E. H. T. Olthof, A. van der Avoird, and P. E. S. Wormer, J. Chem. Phys. **101**, 8430 (1994).